Evolution of Primary and Aggregate Particle-Size Distributions by Coagulation and Sintering

Stavros Tsantilis and Sotiris E. Pratsinis
Dept. of Chemical Engineering, University of Cincinnati, Cincinnati, OH 45221

A sectional model for aggregate aerosol dynamics accounting for gas-phase chemical reaction, coagulation, and sintering at nonisothermal conditions is presented. The aggregate structure was considered by the implementation of a constant mass fractal dimension on the aggregate collision diameter and an average, but variable, aggregate area within a given volume section. The model showed separately the evolution of the size distribution of the primary and aggregate particles. Model predictions with respect to average primary particle diameters and aggregate particle-size distributions were evaluated by comparing with experimental data for synthesis of titania by $TiCl_4$ oxidation in a furnace aerosol flow reactor. The effects from sintering time and mass fractal dimension are also discussed.

Introduction

Aerosol formation of aggregate particles is important in materials production (for instance, synthesis of pigments, fumed silica and alumina, as well as fine nickel and iron, to name a few) and air pollution control (of fly ash and other combustion aerosols). Aggregate particles are clusters of individual (spherical or faceted) particles tightly kept together by a chemical bond. These particles are also known as hard agglomerates (Pratsinis, 1998). Depending on the application, the desired product may be in the form of nonaggregate or aggregate powders. For example, nonaggregate powders are desired in pigments and cosmetics, while aggregate particles of high specific surface areas are required in reinforcing, photocatalysis, and catalysis in general (Pratsinis, 1998). Aggregates are typically formed by coagulation and sintering in aerosol flame reactors. Quantitative understanding (modeling) of aggregate formation is therefore important if experimental setups are to be scaled up and industrial process conditions to be optimized.

Koch and Friedlander (1990) introduced an elegant model describing particle growth by coagulation and sintering. Their model predicted average primary particle sizes, but neglected the effect of aggregate structure on the collision rate by assuming that aggregates collided at the same rate as spherical particles of equal volume. Xiong and Pratsinis (1993) developed an elaborate two-dimensional sectional model incorporating the effect of sintering (Koch and Friedlander, 1990) to the population balance equation. Their model traced particle volume and surface-area evolution for coagulation and sintering from the free molecular to the continuum regime. They related the accessible surface area of an aggregate to its volume through a constant scaling factor and compared model predictions with experimental data on silica, titania, and even boron carbide (Xiong et al., 1993, 1992). A simple monodisperse model to describe the particle morphology, size, and number concentration by coagulation and sintering was proposed by Kruis et al. (1993). In this model the radius of gyration was implemented as the collision radius of aggregates of constant mass fractal dimension. Regarding the primary particle diameter, the model predictions were in agreement, at certain cases, with sectional (Xiong and Pratsinis, 1993), self-preserving (Koch and Friedlander, 1990) models, and experimental data on silicon formation.

Akhtar et al. (1994) developed a Monte Carlo simulation to describe coagulation and sintering of two-dimensional particles. They accounted for particle restructuring through energy minimization, and showed the time evolution of the cluster mass fractal dimension. More specifically, their simulations showed a rather exponential decay of the mass fractal dimension with respect to Monte Carlo time steps (Figure 8 of Akhtar et al., 1994). In addition, the mass fractal dimension seemed to decrease more steeply for low rather than high sintering rates. At longer Monte Carlo times, though, mass fractal dimensions, for both slow and fast sintering, approached a constant value of 1.55, corresponding to that dictated by cluster–cluster aggregation of two-dimensional par-

Correspondence concerning this article should be addressed to S. E. Pratsinis.
Present address of S. E. Pratsinis: Institut für Verfahrenstechik, ETH Zentrum, Zürich 8092, Switzerland.

ticles [also equivalent to $D_f = 1.8$ for three-dimensional particles (Seto et al., 1997)].

Seto et al. (1995) studied the sintering of titania aggregates of nanosized primary particles. By solving the basic equation that accounted for the effect of sintering on the aggregate surface area (Koch and Friedlander, 1990), they explained the experimentally observed results of aggregate densification and primary particle growth within the range of 1,000−1,500 K. Seto et al. (1997) extended their study using a sectional technique (Xiong and Pratsinis, 1993) for polydisperse titania and silica aggregates and found that sintering of primary particles occurred at temperatures that were 50−100% of the bulk melting points of the particle material. Their experimental observations for the sintering rates of silica and titania were in agreement with Xiong et al. (1993) and Kobata et al. (1991), respectively.

Vemury et al. (1994a) addressed simultaneous coagulation and sintering by solving the population-balance equation using the technique of Hounslow et al. (1988). The aggregate structure was taken into consideration by the implementation of a constant mass fractal dimension of 1.8 on the aggregate collision volume. They showed that experimental data (Xiong et al., 1993) could be better explained with this formulation and a modified sintering rate, as they could distinguish between primary and aggregate particle-size distributions.

Lehtinen et al. (1996) proposed an equation for the dimensionless excess area of aggregates and determined the effect of sintering based on the difference between collision and coalescence times. When those two times were equal, dendrites were formed, while the constituent primary particles stopped growing. In addition, they studied the effect of process variables such as temperature, velocity, and volume loading on the size of primary particles in turbulent gas flows in a pipe and turbulent round free jets.

Oh and Sorensen (1997) used light scattering to measure the aggregation rate of fractal-like soot aggregates in a rarified gas. They also measured the radius of gyration, fractal dimension, monomer size, and number of monomers per aggregate. An aggregation kernel valid from the free molecular to the continuum regime was also implemented on the Smoluchowski equation, which was then compared to experimental cluster kinetics. Differences between theory and experiments were attributed to high uncertainties in the refractive index of soot as well as to the attractive dispersive forces among particles.

Rogak (1997) extended the discrete sectional formulation by Wu and Flagan (1988) to study primary particle formation by coagulation with rapid coalescence and condensation-like growth. He assumed instantaneous sintering for particles below some size "D_{melt}" and birth of primary particles above this critical size. His model showed that primary particle diameters were less temperature dependent than would be expected from existing sintering models.

Recent advances in computational resources make sectional models increasingly attractive although they may seem more complex compared to monodisperse or moment techniques. Therefore, the model presented is based on a sectional technique (Vemury et al., 1994a) for simulation of gas phase chemical reaction, coagulation, and sintering of aggregates at nonisothermal conditions. The aggregate structure is considered by implementing a constant mass fractal dimension on the so-called aggregate collision diameter (Kruis et al., 1993). An average but variable aggregate surface area is also used in each section following the results of Xiong and Pratsinis (1993). The model is first validated at certain limiting cases for coagulation of spherical and nonspherical (noncoalescing or nonsintered) fractal-like particles. Model predictions are then compared with experimental data and other existing models for simultaneous coagulation and sintering of titanium dioxide.

Theory

Particles in gases are formed by chemical reaction, coagulation, and sintering in the absence of a nucleation barrier and surface growth, as in aerosol synthesis of fumed silica (Ulrich, 1971) and even of titania (Xiong and Pratsinis, 1991), especially at dilute precursor (that is, $TiCl_4$) concentrations that are typical in laboratory studies (Pratsinis and Spicer, 1998). The rate of change of the aggregate size distribution is given by (Friedlander, 1977):

$$\frac{dn(v)}{dt} = R \cdot \delta(v - v_o) + \frac{1}{2}\int_0^v \beta(\tilde{v}, v - \tilde{v}) \cdot n(\tilde{v}) \cdot n(v - \tilde{v})\, d\tilde{v} - n(v)\int_0^\infty \beta(\tilde{v}, v) \cdot n(\tilde{v})\, d\tilde{v}. \quad (1)$$

The first term in the righthand side (RHS) refers to new particle (monomer) formation by chemical reaction, while the other two RHS terms refer to gain and loss of aggregates of size v by coagulation. Although this equation offers many solutions depending on approximations on the shape of the size distribution, here a sectional technique is used (Hounslow et al., 1988; Vemury et al., 1994a) and applied to synthesis of TiO_2 by $TiCl_4$ oxidation (Akhtar et al., 1991), as there are a lot of data in the open literature and reasonably good documentation of the pertinent material properties.

The aggregate size distribution is discretized in M sections. Specifically, following the sectionalization of Hounslow et al. (1988), each section i is represented by a characteristic aggregate volume $v_i = 2^{(i-1)}v_o$, where v_o is the equivalent spherical volume of a TiO_2 monomer (molecule). In addition, v_i is the average volume of the upper and lower boundary sizes of section i, $v_i = (v_{b,i+1} + v_{b,i})/2$ (Spicer and Pratsinis, 1996). The relation between representative volumes of two consecutive sections is $v_{i+1} = 2v_i$ (spacing factor $f_s = 2$), which is a rather coarse sectionalization but results in a small error of about 3% in the geometric standard deviation of the self-preserving distributions (Table 3 of Vemury et al., 1994b). For a more refined and random discretization pattern, the model of Hounslow et al. (1988) should be modified (Kumar and Ramkrishna, 1996). This modification, however, increases computational requirements substantially.

The number concentration ($\#/g_{\text{gas}}$) of titania monomers (molecules) in the first section is given by

$$\frac{dN_1}{dt} = -\frac{dC_{TiCl_4}}{dt} - \left\{ N_1 \sum_{j=1}^{M} \beta_{1,j} N_j \right\} \rho_g = kC_{TiCl_4} - \left\{ N_1 \sum_{j=1}^{M} \beta_{1,j} N_j \right\} \rho_g, \quad (2)$$

where ρ_g is the gas density (g/cm^3), $\beta_{1,j}$ (cm^3/s) the collision kernel between the monomers and particles of bigger sections, C_{TiCl_4} the concentration of $TiCl_4$ (molecules/g_{gas}), and k (s^{-1}) the oxidation rate constant of $TiCl_4$ (Pratsinis et al., 1990). For the rest of the sections the evolution of the number concentration, N_i, of aggregates per gram of gas is (Hounslow et al., 1988):

$$\frac{dN_i}{dt} = \left\{ N_{i-1} \sum_{j=1}^{i-2} 2^{j-i+1} \beta_{i-1,j} N_j + \frac{1}{2} \beta_{i-1,i-1} N_{i-1}^2 - N_i \sum_{j=1}^{i-1} 2^{j-i} \beta_{i,j} N_j - N_i \sum_{j=i}^{M} \beta_{i,j} N_j \right\} \rho_g. \quad (3)$$

Interparticle forces and nonunity sticking coefficients are neglected. The first RHS term in Eq. 3 refers to the rate of birth of aggregates in section i by collisions between aggregates of the $i-1$ section and j sections ranging from 1 to $i-2$. The second RHS term refers to birth of aggregates in the ith section by collisions of equal size $(i-1)$ aggregates. The third accounts for the death rate of aggregates in section i by collisions between these aggregates and smaller ones. The fourth RHS term corresponds to the death rate of aggregates in section i by collisions between these aggregates and aggregates in the same or higher size intervals.

The present model gives an average primary particle diameter, $d_{p,i}$ (cm), within a given aggregate volume section i, as the primary particle-size distribution within an aggregate is, typically, rather narrow (that is, the constituent particles in an aggregate are considered to have the same diameter). This is a simplification following the approach of Kruis et al. (1993). An indication of the error of the preceding simplification can be derived from the detailed two-dimensional sectional formulation of Xiong and Pratsinis (1993), which shows that the effect of the number of surface-area sections within a given aggregate volume size-interval is quite small ($< 5\%$). Furthermore, the assumption of an average primary and aggregate particle size per section has no effect on the aggregate size distribution. For example, when Vemury et al. (1994b) used an average aggregate particle size per section, their model predictions were nearly identical (error 0.2–0.3% with respect to the geometric standard deviation of the self-preserving size distribution for spacing factor, $f_s = 2$) to those of Landgrebe and Pratsinis (1990), accounting for the full distribution per section (Table 3 of Vemury et al., 1994b).

The effect of sintering on the aggregate surface area is given by (Koch and Friedlander, 1990):

$$\frac{da_i}{dt} = -\frac{1}{\tau_{s,i}} (a_i - a_{s,i}), \quad (4)$$

where a_i (cm^2) is the surface area of an aggregate in section i, $\tau_{s,i}$ is the characteristic sintering time (s) [the time needed to reduce by approximately 63% the excess surface area of an aggregate over that of an equal mass sphere (Xiong and Pratsinis, 1993)], and $a_{s,i}$ is the surface area of a completely fused (spherical) aggregate:

$$a_{s,i} = \left(\frac{v_i}{v_o} \right)^{2/3} a_o. \quad (5)$$

For TiO_2, $\tau_{s,i}$ is given by Xiong et al. (1993):

$$\tau_{s,i} = 8.3 \times 10^{16} d_{p,i}^4 T \exp\left(\frac{3{,}700}{T} \right), \quad (6)$$

or by Kobata et al. (1991):

$$\tau_{s,i} = 7.4 \times 10^{8} d_{p,i}^4 T \exp\left(\frac{31{,}000}{T} \right). \quad (7)$$

For the collision kernels $\beta_{i,j}$, the Fuchs interpolation function for Brownian coagulation in the free molecule and continuum regimes is used (Seinfeld, 1986). Furthermore, the effect of aggregate structure on the collision kernel is incorporated by replacing the primary particle diameter, $d_{p,i}$, with the so-called collision diameter, $d_{c,i}$ (Vemury et al., 1994a):

$$\beta_{i,j} = 2\pi (D_i + D_j)(d_{c,i} + d_{c,j}) \times \left[\frac{d_{c,i} + d_{c,j}}{d_{c,i} + d_{c,j} + 2g_{i,j}} + \frac{8(D_i + D_j)}{c_{i,j}(d_{c,i} + d_{c,j})} \right]^{-1}, \quad (8)$$

where D_i (cm$^2 \cdot$ s^{-1}) is the diffusion coefficient of an aggregate of size i based on the collision diameter, $g_{i,j}$ is the transition parameter, and $c_{i,j}$ has units of velocity (cm/s) as defined in Seinfeld (1986). The collision diameter of an aggregate is given by Kruis et al. (1993):

$$d_{c,i} = d_{p,i} \left(\frac{v_i}{v_{p,i}} \right)^{1/D_f} \quad (9)$$

and

$$d_{p,i} = \frac{6v_i}{a_i}, \quad (10)$$

where $v_{p,i}$ (cm^3) is the volume of a (spherical) primary particle (in section i), and D_f is the so-called mass fractal dimension varying from 1 to 3. As a first approximation, though, a constant mass fractal dimension of 1.8 is commonly used that corresponds to growth by cluster–cluster aggregation. This is common for aggregates generated in high-temperature aerosol processes (Kruis et al., 1993; Seto et al., 1997). In addition, the ratio $(v_i/v_{p,i})$ is equal to the number of primary particles n_i in a representative aggregate in the size interval i, so that when n_i is 1 then $d_{p,i}$ equals $d_{c,i}$. For higher values of n_i, $d_{c,i}$ approaches the radius of gyration of the ith aggregate (Kruis et al., 1993).

The initial aggregate surface area in each section is the maximum one. If a_o is the surface area of a single monomer, the maximum surface area of a representative aggregate in section i will be that of a nonfused (noncoalescing or nonsintered) aggregate *initially* consisting of $2^{(i-1)}$ monomers, that is, $a_o \cdot 2^{(i-1)}$. Hence, *initially* the primary particle diameter $d_{p,i}$ and the monomer diameter d_o coincide. In this way, the initial aggregate surface area values are defined in a clear and straightforward manner, avoiding the use of any adjustable parameters.

Equations 2–4 can be transformed from a Lagrangian to an Eulerian form by

$$\frac{dF}{dt} = \frac{dF}{dx}\frac{dx}{dt} = \frac{dF}{dx}u_x, \tag{11}$$

where $F = N_i$ or C_{TiCl_4} and u_x (cm/s) is the average gas velocity along the aerosol reactor:

$$u_x = \frac{Q_{in}T(x)}{T_{in}S} \tag{12}$$

where Q_{in} (cm^3/s) is the gas-inlet flow rate, T_{in} (K) the inlet temperature, and S (cm^2) is the cross-sectional surface area of the reactor, that is, $T_{in} = 296$ K and $S = 7.91$ cm^2 for Akhtar et al. (1991). The temperature profiles $T(x)$ along the reactor, for different furnace wall temperatures, are given by Akhtar et al. (1991).

The system of Eqs. 2–4 (along with the oxidation rate of $TiCl_4$) can now be solved for each section of the size distribution. For that purpose, a differential equation solver DGEAR (IMSL, 1980) is used (Tsantilis, 1998). Since v_i is fixed and a_i decreases, as dictated by Eq. 4, $d_{p,i}$ will increase, thus denoting the growth of primary particles from monomers. For an initial concentration C_{in} of $TiCl_4$, the *initial* conditions will be: $C_{TiCl_4} = C_{in}$, $N_i = 0$ for $i = 1$ to M, and $a_i = 2^{i-1}a_o$ (or $d_{p,i} = d_o$ at $t = 0$ s) for $i = 1$ to M. The total number of sections used is $M = 40$.

This model constitutes a relatively simple approach to the solution of the population balance equation for simultaneous gas-phase chemical reaction, coagulation, and sintering. As mentioned, the representative volume of each section is the average volume between the lower and upper limits of the corresponding size interval. Since the representative volume in the first section is that of the titania molecule, v_o, lower and upper boundaries are $(2/3)v_o$ and $(4/3)v_o$, respectively. Similarly, boundaries of each section i with a representative volume $v_i = 2^{i-1}v_o$ are $(2^i/3)v_o$ and $(2^{i+1}/3)v_o$. This discretization is necessary to satisfy the mass balance:

$$\text{Mass of } TiO_2\ (g/g_{gas}) = (C_{in} - C_{TiCl_4})v_o\rho_p = \left(\sum_{i=1}^{M} N_i v_i\right)\rho_p. \tag{13}$$

Predictions of this model are compared to experimental data derived by differential mobility particle-size (DMPS) measurements. The characteristic diameter used in the experimental and model-predicted particle-size distributions, is the *aggregate area equivalent diameter*, $d_{s,i} = \sqrt{a_i/\pi}$ (Xiong et al., 1993; Seto et al., 1997). Similarly, the range of each section has to be defined in terms of aggregate area equivalent diameters ($d_{sb,i+1} - d_{sb,i}$), where $d_{sb,i} = \sqrt{a_{b,i}/\pi}$. This range changes with time by sintering, so Eq. 4 also has to be solved for boundaries of each section. Note that since sintering is solely a function of the primary particle diameter and process temperature, and the representative volume in each section is fixed, Eq. 4 can be treated independently. Based on the volume and area discretization mentioned earlier, *initial* (maximum) values for the areas corresponding to the boundaries of each section will be (for $i = 1,\ M+1$):

$$a_{b,i} = 2^{i-1}a_o\left(\frac{2}{3}\right)^{2/3}. \tag{14}$$

Equation 14 stems from the assumption that the smallest volume in the present discretization ($2/3v_o$, lower boundary of the first section) refers to a sphere.

A number of average properties can be calculated from the particle-size distributions. More specifically, the aggregate geometric (number) mean diameter, d_g, is defined as:

$$d_g = \left(\frac{6v_g}{\pi}\right)^{1/3}, \tag{15}$$

where v_g is the aggregate geometric mean volume. The aggregate geometric mean volume is used for the calculation of the geometric standard deviation σ_g (Eqs. B6 and B9 of Landgrebe and Pratsinis, 1990). The aggregate equivalent volume (number) mean diameter, d_v, is

$$d_v = \frac{\sum_{i=2}^{M}\left(\frac{6v_i}{\pi}\right)^{1/3}N_i}{\sum_{i=2}^{M}N_i}. \tag{16}$$

The calculation of d_g and d_v refers to aggregate properties and does not include the first section of the size distribution that corresponds to monomers (that is, single TiO_2 molecules). Furthermore, the primary particle mean diameter, d_{pr} (in the gas stream), is

$$d_{pr} = \frac{\sum_{i=1}^{M} n_i N_i d_{p,i}}{\sum_{i=1}^{M} n_i N_i} = \frac{\sum_{i=1}^{M}\left(\frac{v_i}{v_{p,i}}\right)d_{p,i}N_i}{\sum_{i=1}^{M}\left(\frac{v_i}{v_{p,i}}\right)N_i}. \tag{17}$$

Finally, the dimensionless primary and aggregate particle-size distributions are represented, respectively, by

$$(\Delta n/n_T)/(\Delta \ln d_{pb}) = \left[N_i \cdot n_i \Big/ \left(\sum_{i=1}^{M} N_i \cdot n_i\right)\right] \Big/ (\ln d_{pb,i+1} - \ln d_{pb,i}) \tag{18}$$

$$(\Delta N/N_T)/(\Delta \ln d_{sb}) = \left(N_i \Big/ \sum_{i=1}^{M} N_i\right) \Big/ (\ln d_{sb,i+1} - \ln d_{sb,i}) \tag{19}$$

where $d_{pb,i} = 6 \cdot v_{b,i}/a_{b,i}$ is the primary particle diameter at the lower boundary of section i, n_i is the number of primary particles per single aggregate in section i, n_T is the total number of primary particles in the gas stream (primaries/g_{gas}), and N_T is the total number concentration of aggregates (aggregates/g_{gas}).

Results and Discussion

Model validation

First, the model is validated by comparing its particle-size distribution predictions for simultaneous gas-phase chemical reaction and coagulation of spherical particles (pure coalescence) with the theoretical calculations of Akhtar et al. (1991) (Figure 12 based on Landgrebe and Pratsinis, 1990). The two models are in good agreement (Tsantilis, 1998). It should be noted that the present model is much simpler and faster than those of Landgrebe and Pratsinis (1990) and Xiong and Pratsinis (1993), as it does not integrate in each section (Gelbard and Seinfeld, 1978) and relies on the midpoint of each volume size-interval (Spicer and Pratsinis, 1996). It also should be clarified that there are two ways to account for pure coalescence in the proposed model. One is to solve only Eqs. 2 and 3 and replace the collision diameter in each section by the corresponding representative volume equivalent diameter. The other way is to solve Eqs. 2–4 and set the sintering time to a very small value (10^{-9} s). Both ways give the same results.

For completeness, the present sectional formulation is also validated for coagulation of noncoalescing (or nonsintered) aggregates (pure aggregation) of various constant mass fractal dimensions ($D_f = 1-3$) in the free molecular and continuum regimes (Vemury and Pratsinis, 1995). This is accomplished by using the collision kernels defined in Vemury and Pratsinis (1995) and by either setting the sintering time to a very large value (10^{16} s) or by solving Eqs. 2 and 3 excluding the reaction mode in both cases. The self-preserving size distributions of Vemury and Pratsinis (1995) for a spacing factor $f_s = 2$ as well as the corresponding geometric standard deviations and normalized number concentration decays match those of this model.

Evolution of primary and aggregate particle-size distributions

Figure 1 shows the axial temperature profile of the reactor, the evolution of TiO_2 mass (g/g_{gas}) and dimensionless aerosol total number concentration, N_T/C_{in}, for the experimental conditions of Akhtar et al. (1991): residence time 1.6 s, furnace set temperature, 1,400 K, inlet-gas flow rate Q_{in}, 2.876 L/min, and initial $TiCl_4$ concentration, 1.56×10^{-5} mol/L (defined at 1,400 K). The sintering time is given by Eq. 6. Initially ($t < 0.58$ s) the depletion rate of the $TiCl_4$ precursor is faster than the coagulation rate, thus leading to an increase in the total aerosol number concentration. As soon as the oxidation of the $TiCl_4$ precursor is complete, coagulation becomes dominant and the particle number concentration decreases. However, it is important to see that most of the decay of the particle number concentration takes place before the entrance to the isothermal zone of the furnace reactor.

Figures 2 and 3 show gas-stream primary particle and aggregate size distributions at 0.073 s, 0.58 s, 0.72 s, and 1.6 s, at the same conditions as in Figure 1. At $t = 0.073$ s the depletion of $TiCl_4$ is not yet complete, while the contribution of chemical reaction is more important than that of coagulation. Hence, at $t = 0.073$ s the primary particle and aggregate size distributions coincide, indicating the formation of fully sintered, spherical aggregates (since at small particle sizes sintering is faster than collision rates). At longer times (that is, $t = 0.58$ and 0.72 s) both primary and aggregate size distributions become bimodal (Figures 2 and 3). This is characteristic of the existence of comparable chemical reaction and coagulation modes (Landgrebe and Pratsinis, 1990). More specifically, for $t = 0.58$ s, the primary particle and aggregate size distributions are identical for sizes up to ~20 nm (this can be more obvious when plotting the nonnormalized distributions of N_i, $N_i \cdot n_i$), which is the size range within which aggregates are completely coalesced. In addition, the average aggregate diameter (d_g or d_v) is close to the average primary particle diameter (d_{pr}) for short times, $t \le 0.58$ s (Figure 4),

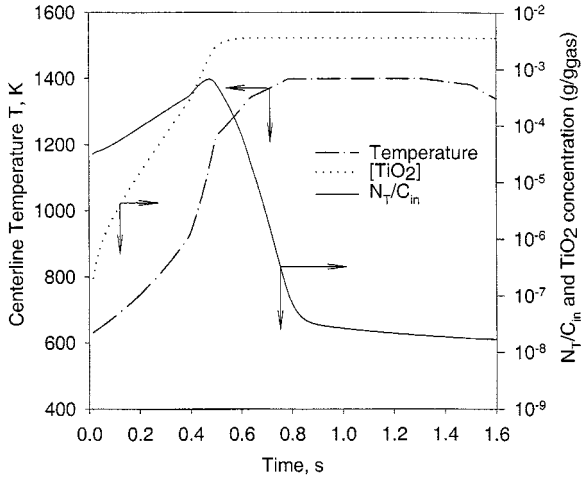

Figure 1. Evolution of temperature, TiO_2 mass (g/g_{gas}), and dimensionless aerosol total number concentration N_T/C_{in} along the reactor.

The residence time is ~1.6 s, the furnace set temperature is 1,400 K, while the inlet gas flow rate Q_{in} and $TiCl_4$ concentration are 2.876 L/min and 1.56×10^{-5} (defined at 1,400 K) mol/L, respectively.

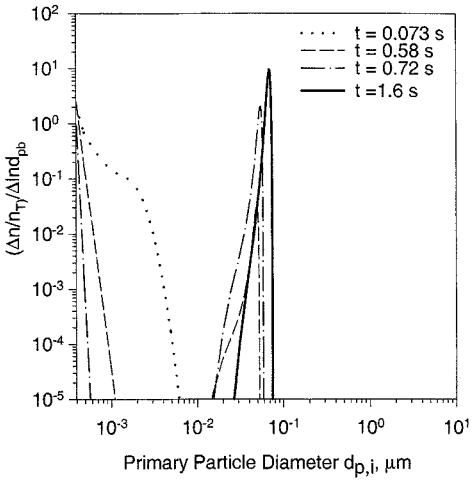

Figure 2. Evolution of the (gas-stream) primary particle-size distribution (PPSD) for the same conditions as in Figure 1.

As the residence time increases, the PPSD becomes narrower by sintering.

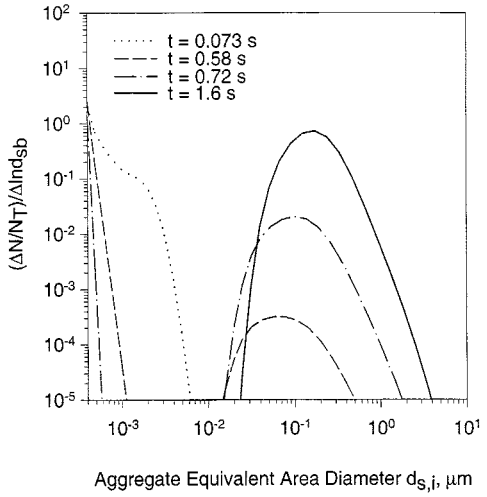

Figure 3. Evolution of the aggregate particle-size distribution (APSD) for the same conditions as in Figure 1.

As the residence time increases, the APSD reaches the self-preserving size distribution for coagulation of fractal-like particles with $D_f = 1.8$.

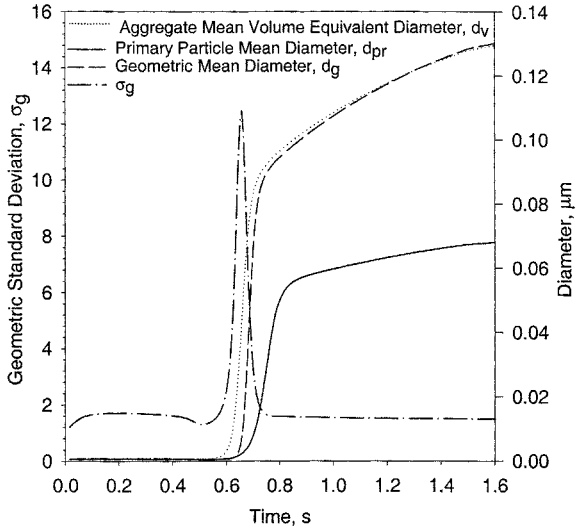

Figure 4. Evolution of the geometric mean diameter d_g and aggregate mean volume equivalent diameter d_v along with the geometric standard deviation σ_g of the aggregate particle-size distribution (APSD) and the primary-particle mean diameter d_{pr} for the same conditions as in Figure 1.

The peak in σ_g corresponds to the bimodal APSD at approximately 0.6 s, which occurs at the end of $TiCl_4$ conversion in the reactor.

implying that the contribution of larger sizes (right parts of both distributions in Figures 2 and 3) is not significant.

The aggregate size distribution becomes wider at a faster rate than that of primary particles, thus accounting for high aggregate collision frequencies with respect to sintering. Experimental data in the literature (Akhtar et al., 1991) indicate that the primary particle-size distribution is generally narrower than that of the aggregates. Here, the calculated geometric standard deviations of the primary and aggregate particle-size distributions reach asymptotically the values of 1.06 and 1.49, respectively, at $t = 1.6$ s. The bigger the primary particles grow, the larger is their characteristic sintering time. As soon as a critical primary particle size is reached (for the conditions of Figure 1, this size is approximately 60 nm), sintering becomes very slow, obstructing the growth of the primary particle-size distribution. This is elucidated in Figure 2 by observing the sharp right ends of the primary particle-size distributions and the evolution of d_{pr} (Figure 4). At the same time, smaller primary particles gain size and consequently start to sinter at lower rates. This process leads to narrow primary particle-size distributions that are typically observed by scanning electron microscopy (Figure 5 of Akhtar et al., 1991). However, it should be noted that for sintering mechanisms in which the sintering rate is not inversely proportional to particle size, the preceding process will not be as effective. Finally, for 0.87 s $< t <$ 1.6 s there is no chemical reaction and the rate of decrease of N_T/C_{in} dramatically slows down. At $t = 1.6$ s, the aggregate size distribution is unimodal with a lognormal type of shape indicative of the attainment of the self-preserving distribution (Figure 3).

Figure 4 depicts the evolution of the geometric mean diameter, d_g, and aggregate mean volume equivalent diameter, d_v, along with the geometric standard deviation of the aggregate size distribution, σ_g, and the primary particle mean diameter, d_{pr}, for the conditions of Figure 1. The evolution of the integral properties just mentioned summarizes the conclusions reached in Figures 2 and 3. The geometric standard deviation exhibits a maximum at the same region where there is a steep increase in the aggregate and primary-particle mean diameters (d_g, d_v, and d_{pr}) and an equally sharp decrease in $TiCl_4$ concentration. This is also observed by Landgrebe and Pratsinis (1990, figures 6c and 8c), and it is characteristic of a bimodal type of particle-size distribution with the so-called reaction and coagulation modes containing molecular clusters (of size $\lesssim 10^{-3}$ μm) and larger particles (of sizes between $\sim 2\times10^{-2}$ and ~ 1 μm), respectively. For $t > 0.72$ s the geometric standard deviation slowly but steadily decreases to an asymptotic value of 1.49, approaching the self-preserving size distribution. For $t < 0.58$ s the aggregate size is very close to the primary particle size ($d_g \approx d_v \approx d_{pr}$). This denotes that a major part of the distribution is occupied by tiny rather spherical particles. The gap between d_v and d_{pr} is representative of the average number of primary particles per aggregate. As soon as the oxidation of the precursor is complete, aggregates consisting of a large number of primary particles are produced. The initially small primary particles sinter fast under the relatively high temperatures between 0.62 and 0.87 s. At about 0.87 s the temperature inside the reactor reaches its maximum value, while the average primary particle diameter seems to have attained a critical size (approximately 60 nm) above which growth by sintering is slow. Finally, at the exit of the furnace the average number of primary particles per aggregate is approximately 7.

Effect of sintering rate and fractal dimension

Figure 5 shows model predictions for coagulation of spherical particles (broken line), coagulation of fractal-like ($D_f =$

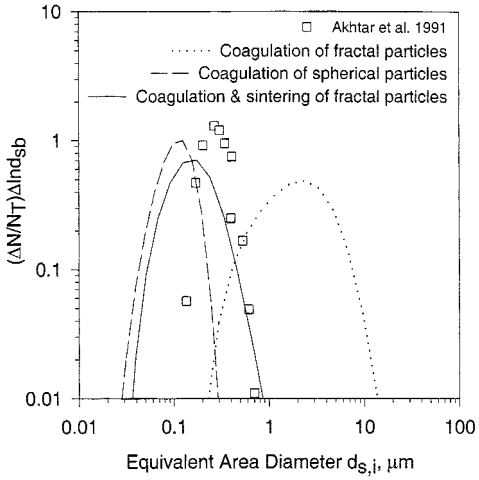

Figure 5. Particle-size distributions predicted by assuming coagulation of spherical particles (– – –), coagulation of fractal-like particles ($D_f = 1.8$) (· · · ·) and concurrent coagulation and sintering of fractal like particles (——) for the conditions of Figure 1.

Clearly, sintering gives a more realistic picture of the process, bringing in a better agreement with the corresponding experimental data of Akhtar et al. (1991).

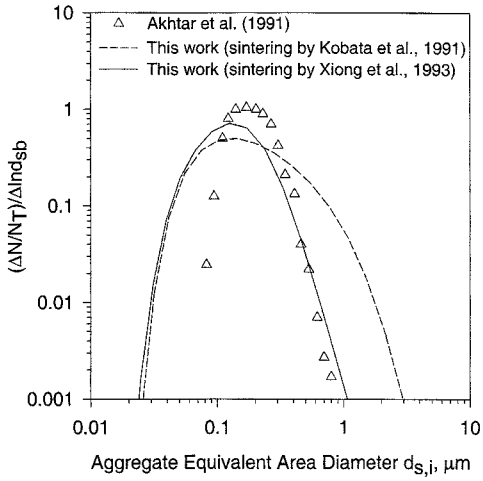

Figure 6. Model predictions of aggregate particle-size distributions using two sintering rates, and comparison with experimental data for residence time ~1.6 s, furnace set temperature 1,400 K, inlet gas flow rate Q_{in}, and $TiCl_4$ concentration 2.674 L/min and 9.34×10^{-6} (defined at 1,400 K) mol/L, respectively.

At this temperature, using the sintering rate by Kobata et al. (1991) gives larger aggregates than by using the effective sintering rate of Xiong et al. (1993).

1.8) particles (dotted line), and concurrent coagulation and sintering of fractal-like ($D_f = 1.8$) particles (solid line), at $t =$ 1.6 s along with experimental data from Akhtar et al. (1991, figure 8) for the conditions of Figure 1. First, assuming perfectly spherical particles gives the narrowest particle-size distribution (broken line in Figure 5), which agrees with Vemury and Pratsinis (1995, figure 3) in the free molecular regime. On the other extreme, neglecting the role of sintering after collision overpredicts the size distribution (dotted line). Accounting for coagulation and sintering gives a distribution between these two cases and comes closest to the measured size distributions (solid line). Especially good agreement is seen on the right tail of the particle-size distribution, while disagreement on the left tail should be attributed to experimental limitations such as losses of finer particles during dilution (Akhtar et al., 1991). For pure coalescence the sintering time approaches zero, while for pure aggregation it approaches infinity. Those two extreme cases are the limits of the proposed model. Sintering is the linking bridge between them. As sintering time increases, it tends to broaden the particle-size distribution and shift it to larger size scales. Low sintering rates lead to bigger aggregates, which grow faster in the free-molecular-transition regime (Akhtar et al., 1991; Otto et al., 1994), shifting the particle-size distribution to the right.

The effect of constant mass fractal dimension on the aggregate size distribution, for simultaneous coagulation and sintering, was also investigated (Tsantilis, 1998). At higher D_f, the distribution shifted to smaller particle sizes, approaching the size distribution of spherical particles (Figure 5). There was no significant change on the geometric standard deviation, however, and the shift of size distribution was not very big, even for D_f equal to 3. It should be clarified that the case of $D_f = 3$ was not equivalent to pure coalescence, since the value of sintering time was still finite (Eq. 6). At mass fractal dimensions higher than 1.8, the shape of the aggregates was more compact and the rate at which collisions occurred diminished, forcing the size distribution to smaller sizes. Finally, the model predictions were closer to experimental data for $D_f = 1.8$ (Tsantilis, 1998).

Figure 6 shows how the predictions of the present model compare to experimental data (Akhtar et al., 1991) for two sintering rates, at residence time ~1.6 s; furnace set temperature 1,400 K; inlet-gas flow rate Q_{in}, 2.674 L/min; and initial $TiCl_4$ concentration, 9.34×10^{-6} mol/L (defined at 1,400 K). For the current reactor temperature profile (Figure 1), the sintering rate by Kobata et al. (1991) is slower than the effective one (Xiong et al., 1993), thus giving rise to larger aggregates consisting of smaller primary particles. For growth in the free-molecular and transition regime ($Kn_g \approx 7$), the bigger the aggregates are the faster the coagulation rate is and the wider the resulting particle-size distribution becomes (Otto et al., 1994). The sintering time proposed by Kobata et al. (1991) explains fairly well experimental data where the initial particle-size range is always bigger than 10 nm (Seto et al., 1995). In the present analysis, however, the smallest size considered is the molecular diameter of TiO_2. The effective sintering rate proposed by Xiong et al. (1993) is in better agreement with experimental data, as its derivation is based on the process conditions. Nevertheless, for higher process temperatures the model predictions (with respect to aggregate size distributions) for both sintering times get closer. This is shown, for instance, in Figure 7 for residence time 1.6 s; furnace set temperature 1,723 K; inlet-gas flow rate, Q_{in}, approximately 2.35 L/min; and inlet $TiCl_4$ concentration 1.16×10^{-5} mol/L (defined at 1,723 K).

In addition to the experimental conditions mentioned earlier, the proposed model was tested for different inlet $TiCl_4$

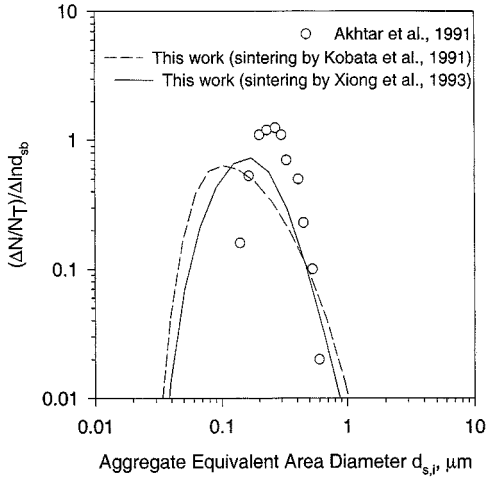

Figure 7. Model predictions of aggregate particle-size distributions using two sintering rates, and comparison with experimental data for residence time 1.6 s, furnace set temperature 1,723 K, inlet gas flow rate Q_{in}, and $TiCl_4$ concentration ~ 2.35 L/min and 1.16×10^{-5} (defined at 1,723 K) mol/L, respectively.

At this high temperature there is little difference in the model predictions regardless of the employed sintering rate.

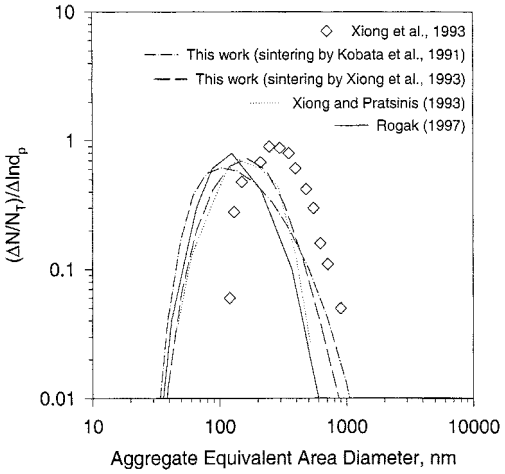

Figure 8. Predicted aggregate particle-size distributions from literature models and from this work for two sintering rates, as well as experimental data for residence time 1.6 s, furnace set temperature 1,700 K, and inlet $TiCl_4$ concentration 1.16×10^{-5} (defined at 1,700 K) mol/L.

concentrations, residence times, and furnace set temperatures (Tsantilis, 1998). In all cases, the mass fractal dimension was set equal to 1.8. The model predicted the same trends as in the experimental results (figures 8 and 9 of Akhtar et al., 1991). Thus, for example, the geometric mean diameter decreased and the standard deviation increased with decreasing inlet precursor concentration or residence time. Furthermore, the model always predicted wider size distributions (the predicted geometric standard deviations were approximately 10% larger than the experimental ones), with a relatively good match at large particle-size scales (Tsantilis, 1998). This might have been an indication of the need for the consideration of particle diffusion in the reactor and sampling (dilution). Such an effect could decrease the population of small particles more, since they could diffuse faster than bigger ones.

According to Akhtar et al. (1992), increasing furnace process temperatures increases the average aggregate size and primary particle diameters. The degree of aggregation, qualitatively defined by the ratio of the DMPS aggregate to BET primary particle diameter, also slightly increases (table 1 of Akhtar et al., 1992). The proposed model predicts the same trend for furnace temperatures of 1,300 K, 1,500 K, 1,700 K, and inlet precursor concentration and residence time of 1.16×10^{-5} mol/L and 1.6 s, respectively (Figures 8 and 10 of Xiong et al., 1993). The experimental BET grain (primary particle) sizes are 0.054, 0.058, and 0.063 μm (figure 8 of Xiong et al., 1993). The corresponding values predicted by the present model and the effective sintering time (Xiong et al., 1993) are 0.065, 0.07, and 0.073 μm. These numbers show that the model slightly overpredicts the average primary particle diameter. The corresponding values predicted by the present model and the sintering time of Kobata et al. (1991) are 0.04, 0.07 and 0.111 μm, which are also in fairly close agreement with Xiong et al. (1993, figure 8, solid line).

Figure 8 compares the predictions of the present model for aggregate size distributions with those of the two-dimensional one by Xiong and Pratsinis (1993) and those by Rogak (1997) for reactor-set temperature 1,700 K, precursor concentration 1.16×10^{-5} (defined at 1,700 K) mol/L, and residence time 1.6 s (Xiong et al., 1993). Experimental data and predictions of the present model are shown for both sintering rates of Kobata et al. (1991) and Xiong et al. (1993), as these are used by Rogak (1997) and Xiong et al. (1993), respectively. As already shown by Xiong et al. (1993) and Rogak (1997), there is deviation between model predictions and the experimental data set. At this rather high temperature the sintering rate has little effect on the model predictions, as is also shown in Figure 7. Clearly, there is little difference among all model predictions, indicating that the present model performs as well as some of the more computationally intensive ones. Finally, it is worth noting that for the conditions studied (Tsantilis, 1998), the proposed model runs in less than 1 h in a Sun Ultra-Sparc 2 workstation.

Conclusions

A simple sectional model was developed describing the evolution of primary and aggregate size distributions for particle synthesis by gas-phase chemical reaction, coagulation, and sintering. The model is quite simple, as it only uses the midpoint values of particle-size sections, reducing substantially the computational effort at little cost of accuracy (less than 3% in the geometric standard deviation of the self-preserving distribution). Each aggregate is characterized by an average but variable surface area, giving a single but variable primary particle-size per aggregate.

The model was applied here to aerosol synthesis of TiO_2 by $TiCl_4$ oxidation in a hot wall reactor. It was shown that primary particles evolve to size distributions substantially narrower than those of the aggregate particles, as sintering is

quite slow for larger primary particle sizes. Further, coagulation and sintering result in a distribution of fractal-like particles ($D_f = 1.8$) that is larger and wider than that of spherical particles, but narrower and smaller than those of fractal-like particles undergoing only coagulation but not sintering.

Model predictions were compared to experimental aggregate size distributions and used to evaluate sintering rates of titania. At high temperatures the choice of sintering rate has little effect on the predicted aggregate size distribution, although significant deviations can be found at low temperatures. Predictions of the model agreed well with those of more computationally intensive ones. Models that account for the detailed fluid and particle dynamics are needed to compare more rigorously with experimental data and to evaluate sintering rates.

Acknowledgments

This work was supported in part by U.S. National Science Foundation Grant CTS-9619392, and in part by the Swiss National Science Foundation. We acknowledge stimulating discussions with Dr. M. K. Akhtar from Millenium Chemicals Inc., and suggestions made by the journal referees.

Notation

$a_{b,i}$ = aggregate area corresponding to the boundaries of each section, cm^2
a_o = molecular surface area of TiO_2, cm^2
$d_{sb,i}$ = aggregate equivalent-area diameter at the lower boundary of section i, cm
M = total number of volume size-intervals
$n(v)$ = size distribution function, cm^{-6}
ρ_p = TiO_2 particle density, g/cm^3

Literature Cited

Akhtar, M. K., Y. Xiong, and S. E. Pratsinis, "Vapor Synthesis of Titania Powder by Titanium Tetrachloride Oxidation," *AIChE J.*, **37**, 1561 (1991).

Akhtar, M. K., S. E. Pratsinis, and S. V. R. Mastrangelo, "Dopants in Vapor Phase Synthesis of Titania Powders," *J. Amer. Ceram. Soc.*, **75**, 3408 (1992).

Akhtar, M. K., G. G. Lipscomb, and S. E. Pratsinis, "Monte Carlo Simulation of Particle Coagulation and Sintering," *Aerosol Sci. Technol.*, **21**, 83 (1994).

Friedlander, S. K., *Smoke, Dust and Haze*, Wiley, New York (1977).

Gelbard, F., and J. H. Seinfeld, "Numerical Solution of the Dynamic Equation for Particulate Systems," *J. Comput. Phys.*, **28**, 357 (1978).

Hounslow, M. J., R. L. Ryall, and V. R. Marshall, "A Discretized Population Balance for Nucleation, Growth and Aggregation," *AIChE J.*, **34**, 1821 (1988).

IMSL, *User's Manual*, Vol. 2, Version 1.1, IMSL Math/Library, Houston, TX (1989).

Kobata, A., K. Kusakabe, and S. Morooka, "Growth and Transformation of TiO_2 Crystallites in Aerosol Reactor," *AIChE J.*, **37**, 347 (1991).

Koch, W., and S. K. Friedlander, "The Effect of Particle Coalescence on the Surface Area of a Coagulating Aerosol," *J. Colloid Interface Sci.*, **140**, 419 (1990).

Kruis, F. E., K. A. Kusters, and S. E. Pratsinis, "A Simple Model for the Evolution of the Characteristics of Aggregate Particles Undergoing Coagulation and Sintering," *Aerosol Sci. Technol.*, **19**, 514 (1993).

Kumar, S., and D. Ramkrishna, "On the Solution of Population Balance Equations by Discretization—I. A Fixed Pivot Technique," *Chem. Eng. Sci.*, **51**, 1311 (1996).

Landgrebe, J., and S. E. Pratsinis, "A Discrete-Sectional Model for Particulate Production by Gas-Phase Chemical Reaction and Aerosol Coagulation in the Free-Molecular Regime," *J. Colloid Interface Sci.*, **139**, 63 (1990).

Lehtinen, K. E., R. S. Windeler, and S. K. Friedlander, "Prediction of Nanoparticle Size and the Onset of Dendrite Formation Using the Method of Characteristic Times," *J. Aerosol Sci.*, **27**, 883 (1996).

Oh, C., and C. M. Sorensen, "Light Scattering Study of Fractal Cluster Aggregation Near the Free Molecular Regime," *J. Aerosol Sci.*, **28**, 937 (1997).

Otto, E., F. Stratmann, H. Fissan, S. Vemury, and S. E. Pratsinis, "Quasi-Self-Preserving Log-Normal Size Distributions in the Transition Regime," *Part. Part. Syst. Charact.*, **11**, 359 (1994).

Pratsinis, S. E., "Flame Synthesis of Ceramic Powders," *Prog. Energy Combust. Sci.*, **24**, 197 (1998).

Pratsinis, S. E., H. Bai, P. Biswas, M. Frenklach, and S. V. R. Mastrangelo, "Kinetics of Titanium[IV]Chloride Oxidation," *J. Amer. Ceram. Soc.*, **73**, 2158 (1990).

Pratsinis, S. E., and P. T. Spicer, "Competition Between Gas Phase and Surface Oxidation of $TiCl_4$ During Synthesis of TiO_2 Particles," *Chem. Eng. Sci.*, **53**, 1861 (1998).

Rogak, S. N., "Modeling Small Cluster Deposition on the Primary Particles of Aerosol Agglomerates," *Aerosol Sci. Tech.*, **26**, 127 (1997).

Seinfeld, J. H., *Atmospheric Chemistry and Physics of Air Pollution*, Wiley, New York (1986).

Seto, T., M. Shimada, and K. Okuyama, "Evaluation of Sintering of Nanometer-Sized Titania Using Aerosol Method," *Aerosol Sci. Technol.*, **23**, 183 (1995).

Seto, T., A. Hiroshita, T. Fujimoto, M. Shimada, and K. Okuyama, "Sintering of Polydisperse Nanometer-Sized Agglomerates," *Aerosol Sci. Technol.*, **27**, 422 (1997).

Spicer, P. T., and S. E. Pratsinis, "Coagulation and Fragmentation: Universal Steady-State Particle-Size Distribution," *AIChE J.*, **42**, 1612 (1996).

Tsantilis, S., "Simulation of Synthesis of Nanosized Particles via the Aerosol Route," MS Thesis, College of Engineering, Univ. of Cincinnati, Cincinnati, OH (1998).

Ulrich, G. D., "Theory of Particle Formation and Growth in Oxide Synthesis Flames," *Combust. Sci. Technol.*, **4**, 47 (1971).

Vemury, S., K. A. Kusters, and S. E. Pratsinis, "Modeling of Coagulation and Sintering of Particles," Preprints, AIChE, New York, *Proc. Int. Particle Technol. Forum*, Denver, **2**, 350 (Aug. 17–19, 1994a).

Vemury, S., K. A. Kusters, and S. E. Pratsinis, "Time-Lag for Attainment of the Self-Preserving Particle-Size Distribution by Coagulation," *J. Colloid Interface Sci.*, **165**, 53 (1994b).

Vemury, S., and S. E. Pratsinis, "Self-Preserving Size Distributions of Agglomerates," *J. Aerosol Sci.*, **26**, 175 (1995).

Wu, J. J., and R. C. Flagan, "A Discrete-Sectional Solution to the Aerosol Dynamic Equation," *J. Colloid Interface Sci.*, **123**, 339 (1988).

Xiong, Y., and S. E. Pratsinis, "Gas Phase Production of Particles in Reactive Turbulent Flows," *J. Aerosol Sci.*, **22**, 637 (1991).

Xiong, Y., and S. E. Pratsinis, "Formation of Agglomerate Particles by Coagulation and Sintering: I. A Two-Dimensional Solution of the Population Balance Equation," *J. Aerosol Sci.*, **24**, 283 (1993).

Xiong, Y., M. K. Akhtar, and S. E. Pratsinis, "Formation of Agglomerate Particles by Coagulation and Sintering: II. The Evolution of the Morphology of Aerosol-Made Titania, Silica and Silica-Doped Titania Powders," *J. Aerosol Sci.*, **24**, 301 (1993).

Xiong, Y., S. E. Pratsinis, and A. W. Weimer, "Modeling the Formation of Boron Carbide Particles in an Aerosol Flow Reactor," *AIChE J.*, **38**, 1685 (1992).

Manuscript received Dec. 4, 1998, and revision received Sept. 21, 1999.